

Supporting Information

External field control and characteristic quantities of Rashba spin orbit coupling in MA_2Z_4 derived monolayer materials

Geng Yong Du,^{ab} Gui-bo Zheng,^{cde} Ying Xu,^{*ab} Wen Zhe Zhou,^{cde} Zhi-Min Ao,^f Wei Sheng,^{ab} and Fang Ping OuYang^{*cde}

a.School of Physics and Electronic Science, Hunan University of Science and Technology, Xiangtan 411201, China

b.Hunan Provincial Key Laboratory of Intelligent Sensors and Advanced Sensor Materials, Xiangtan 411201, Hunan, China

c.School of Physics, Institute of Quantum Physics, Hunan Key Laboratory for Super-Microstructure and Ultrafast Process, and Hunan Key Laboratory of Nanophotonics and Devices, Central South University, Changsha 410083, China

d.School of Physics Science and Technology, and Xinjiang Key Laboratory of Solid-State Physics and Devices, Xinjiang University, Urumqi 830046, China

e.State Key Laboratory of Powder Metallurgy, and Powder Metallurgy Research Institute, Central South University, Changsha 410083, China

f.Advanced Interdisciplinary Institute of Environment and Ecology, Guangdong Provincial Key Laboratory of Wastewater Information Analysis and Early Warning, Beijing Normal University, Zhuhai 519087, China

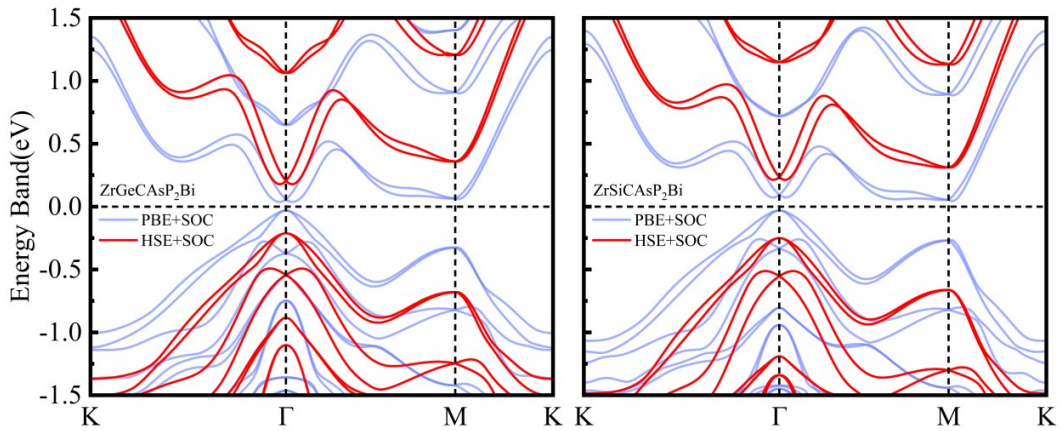


Figure S1. Band structures of several materials in MA_2Z_4 under PBE+SOC and HSE+SOC.

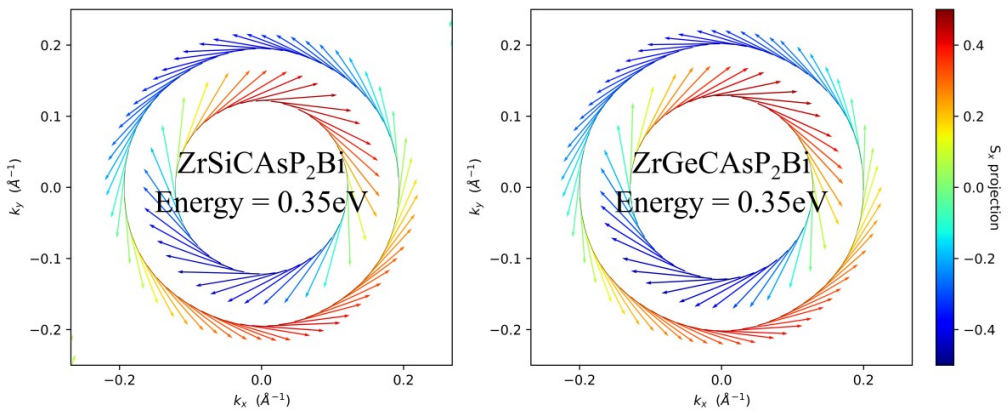
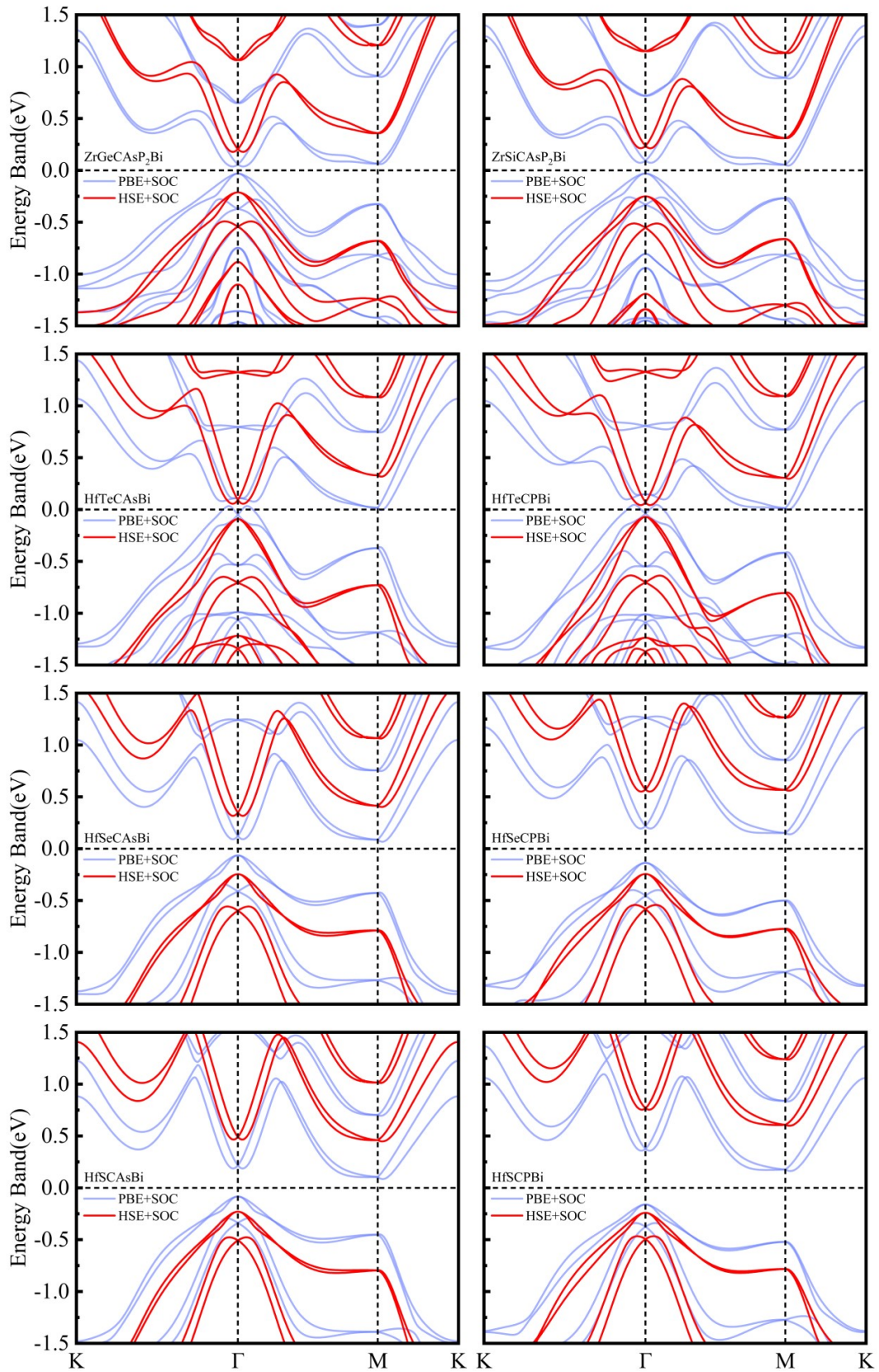
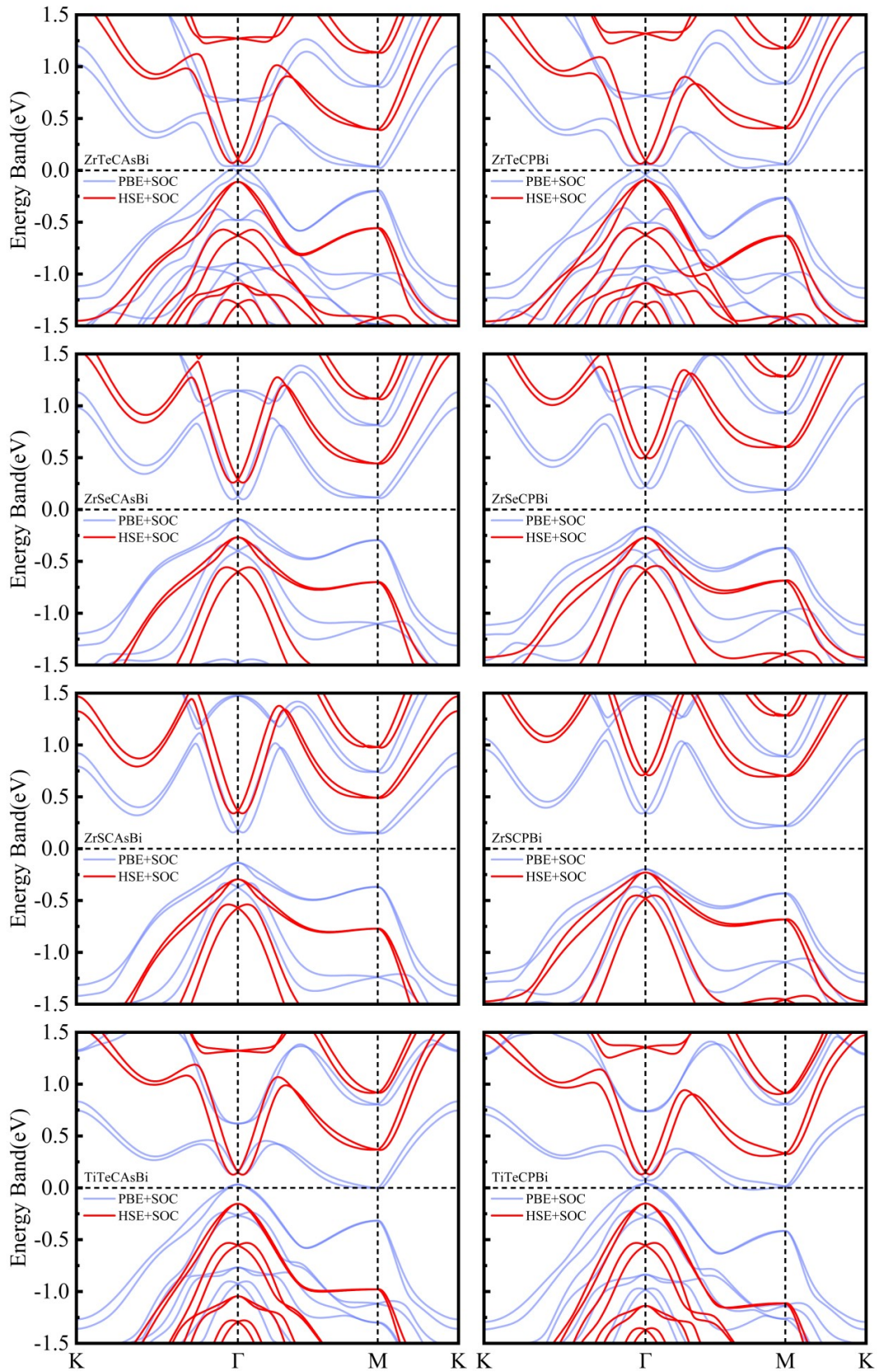


Figure S2. Spin texture diagrams of several materials in MA_2Z_4 at their respective energies (referenced to the Fermi level).





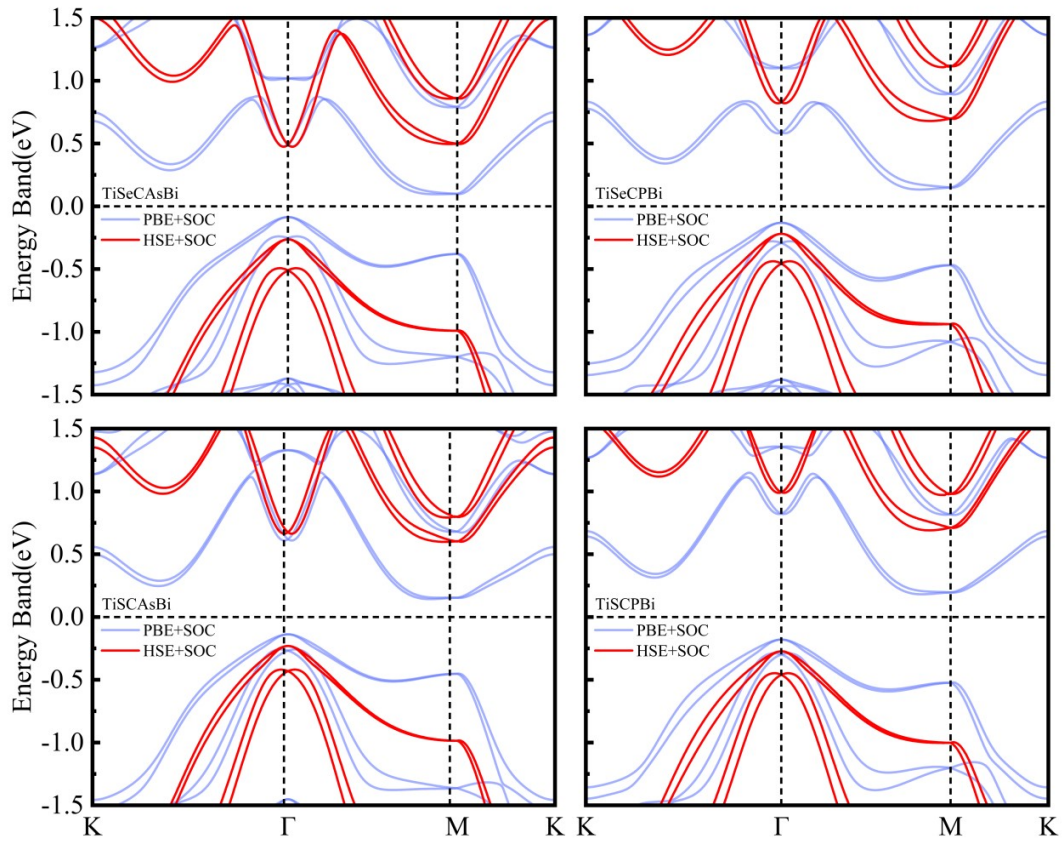
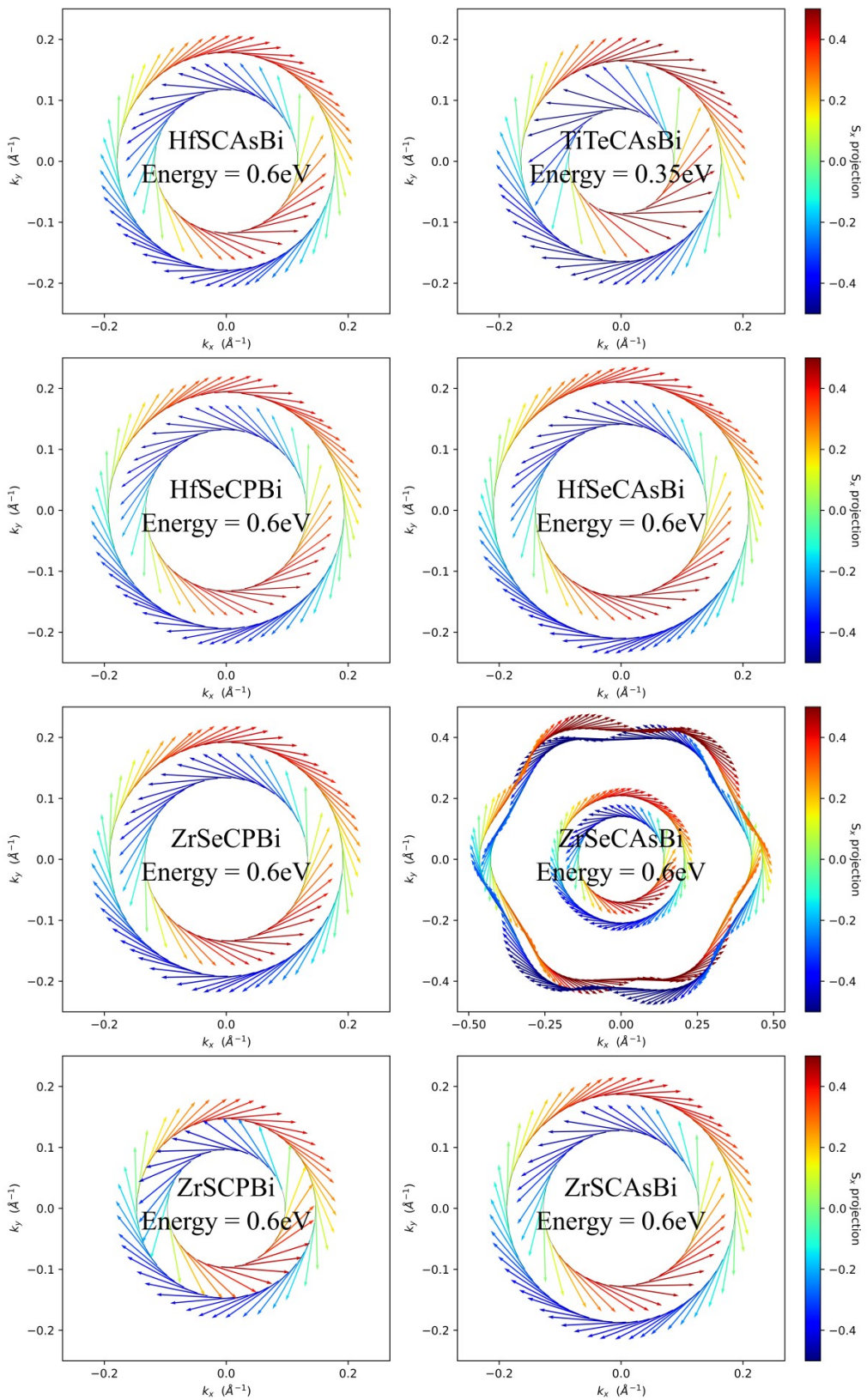


Figure S3. Band structures of several materials in MXAZ₂ under PBE+SOC and HSE+SOC.



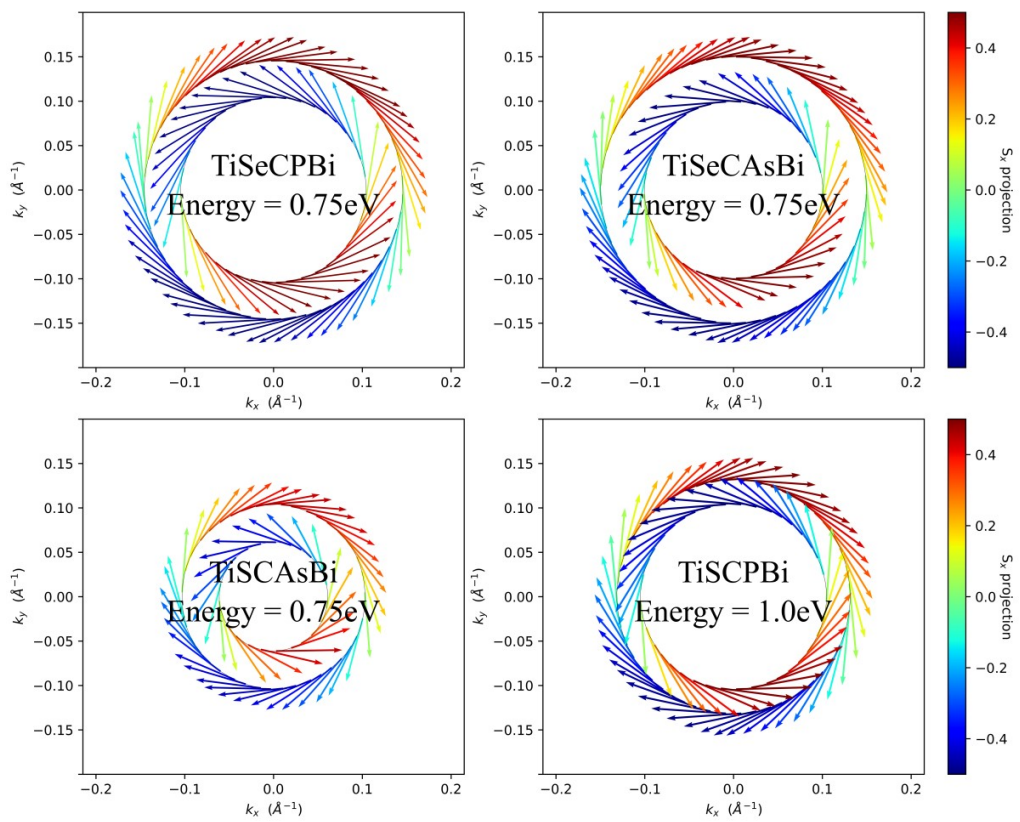
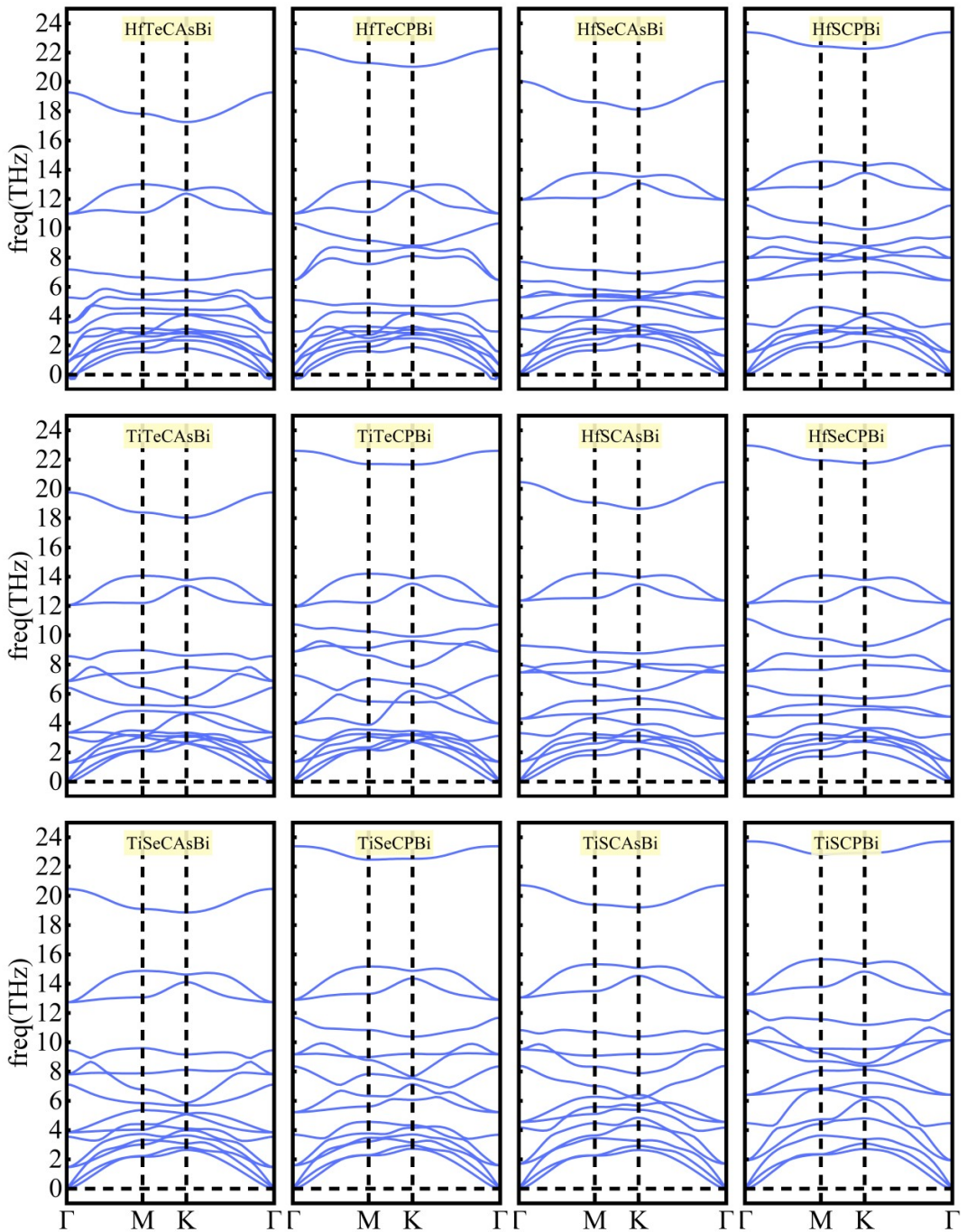


Figure S4. Spin texture diagrams of several materials in MXAZ₂ at their respective energies (referenced to the Fermi level).



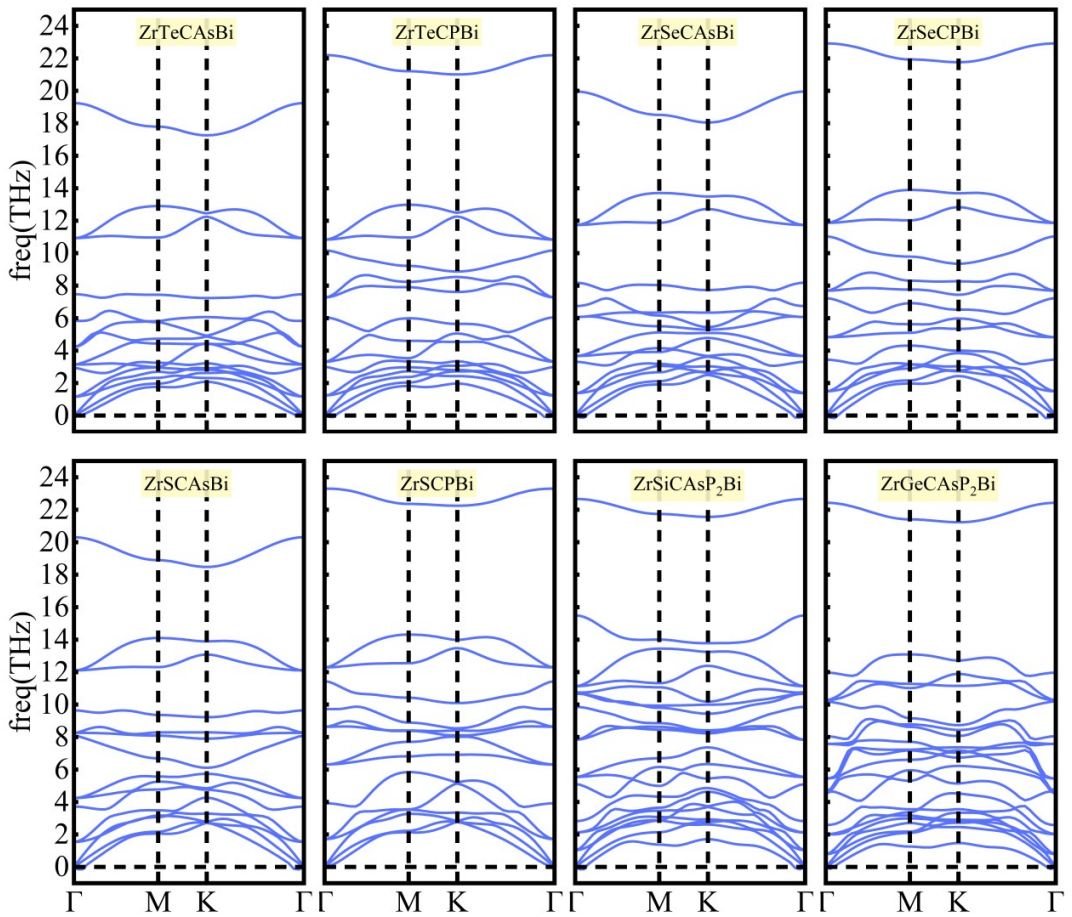
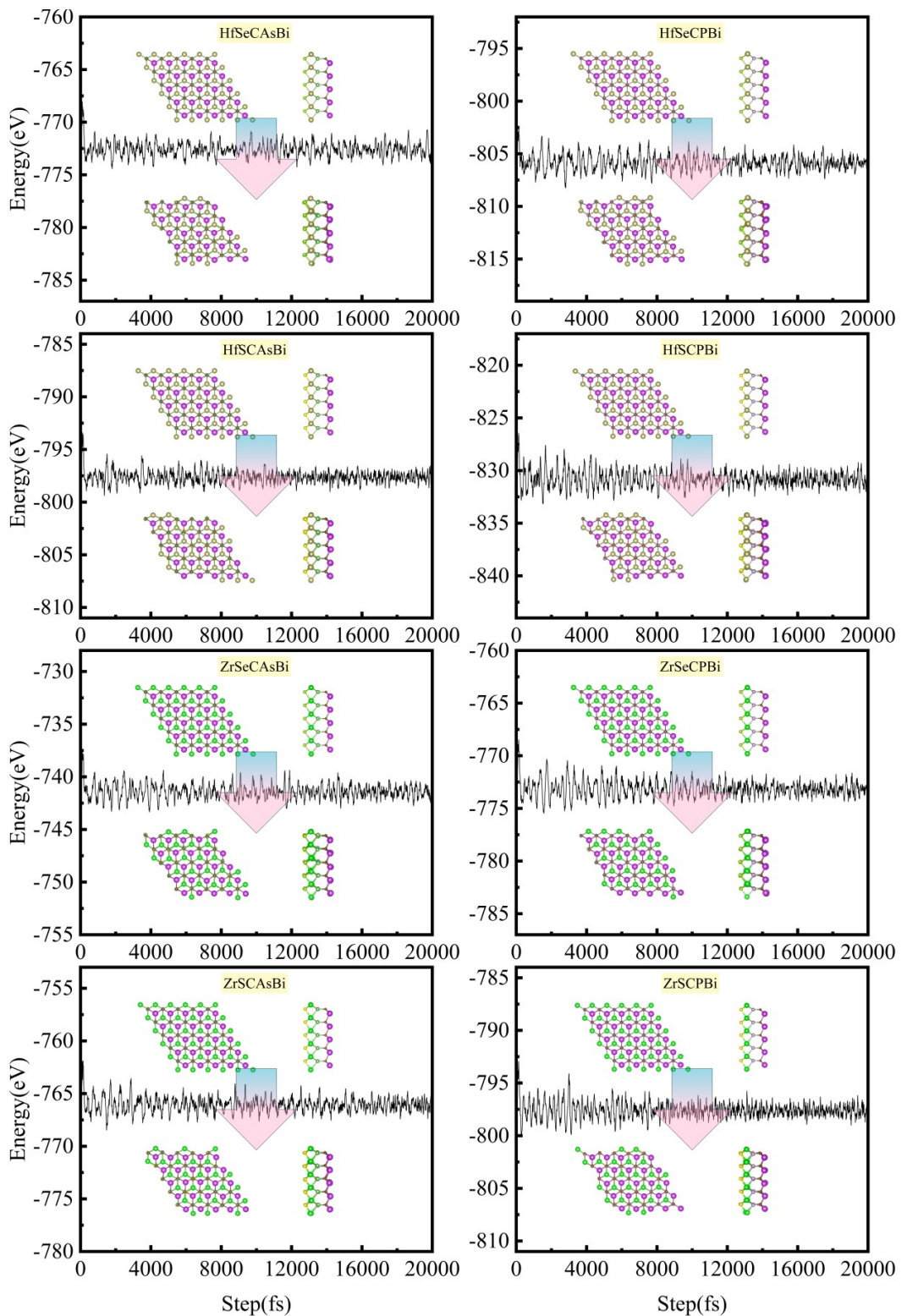


Figure S5. Phonon spectra of several materials in MA_2Z_4 and $MXAZ_2$.



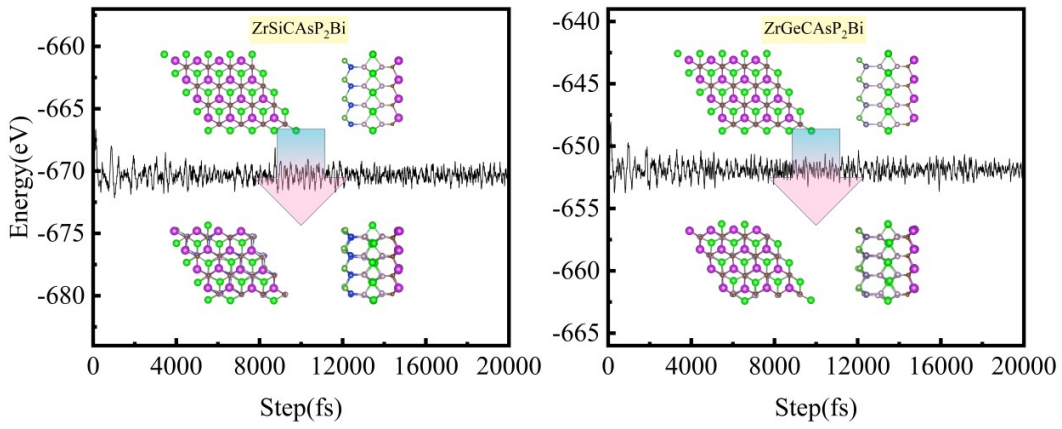


Figure S6. Molecular dynamics simulations of several materials in MA_2Z_4 and MXAZ_2 at 400K.

TABLE S1. The Rashba strength α_R of various materials, the difference in work function between the two sides of the material $\Delta\Phi$, the dipole moment μ within the material, Z represents the sum of atomic numbers, and the electronegativity χ of atoms at different positions.

Material	α_R (eV \AA)	$\Delta\Phi$ (V)	μ (e \AA)	Z	χM (kJ/mol)	χX (kJ/mol)	$\chi Z1$ (kJ/mol)
HfTeCasBi	2.083	1.061	-0.0739	246	1.30	2.10	2.18
HfTeCPBi	1.775	1.268	-0.0865	228	1.30	2.10	2.19
HfSeCasBi	1.847	1.275	-0.0851	228	1.30	2.55	2.18
HfSeCPBi	1.380	1.487	-0.0973	210	1.30	2.55	2.19
HfSCAsBi	1.631	1.419	-0.0931	210	1.30	2.58	2.18
HfSCPBi	1.144	1.602	-0.1023	192	1.30	2.58	2.19
ZrTeCasBi	2.072	1.118	-0.0783	214	1.33	2.10	2.18
ZrTeCPBi	1.749	1.322	-0.0908	196	1.33	2.10	2.19
ZrSeCasBi	1.849	1.348	-0.0912	196	1.33	2.55	2.18
ZrSeCPBi	1.346	1.494	-0.0988	178	1.33	2.55	2.19
ZrSCAsBi	1.668	1.429	-0.0942	178	1.33	2.58	2.18
ZrSCPBi	1.133	1.609	-0.1040	160	1.33	2.58	2.19
TiTeCasBi	1.667	1.19	-0.0780	196	1.54	2.10	2.18
TiTeCPBi	1.360	1.341	-0.0860	178	1.54	2.10	2.19
TiSeCasBi	1.253	1.384	-0.0869	178	1.54	2.55	2.18
TiSeCPBi	0.781	1.591	-0.0983	160	1.54	2.55	2.19
TiSCAsBi	1.030	1.623	-0.0994	160	1.54	2.58	2.18
TiSCPBi	0.552	1.788	-0.1073	142	1.54	2.58	2.19

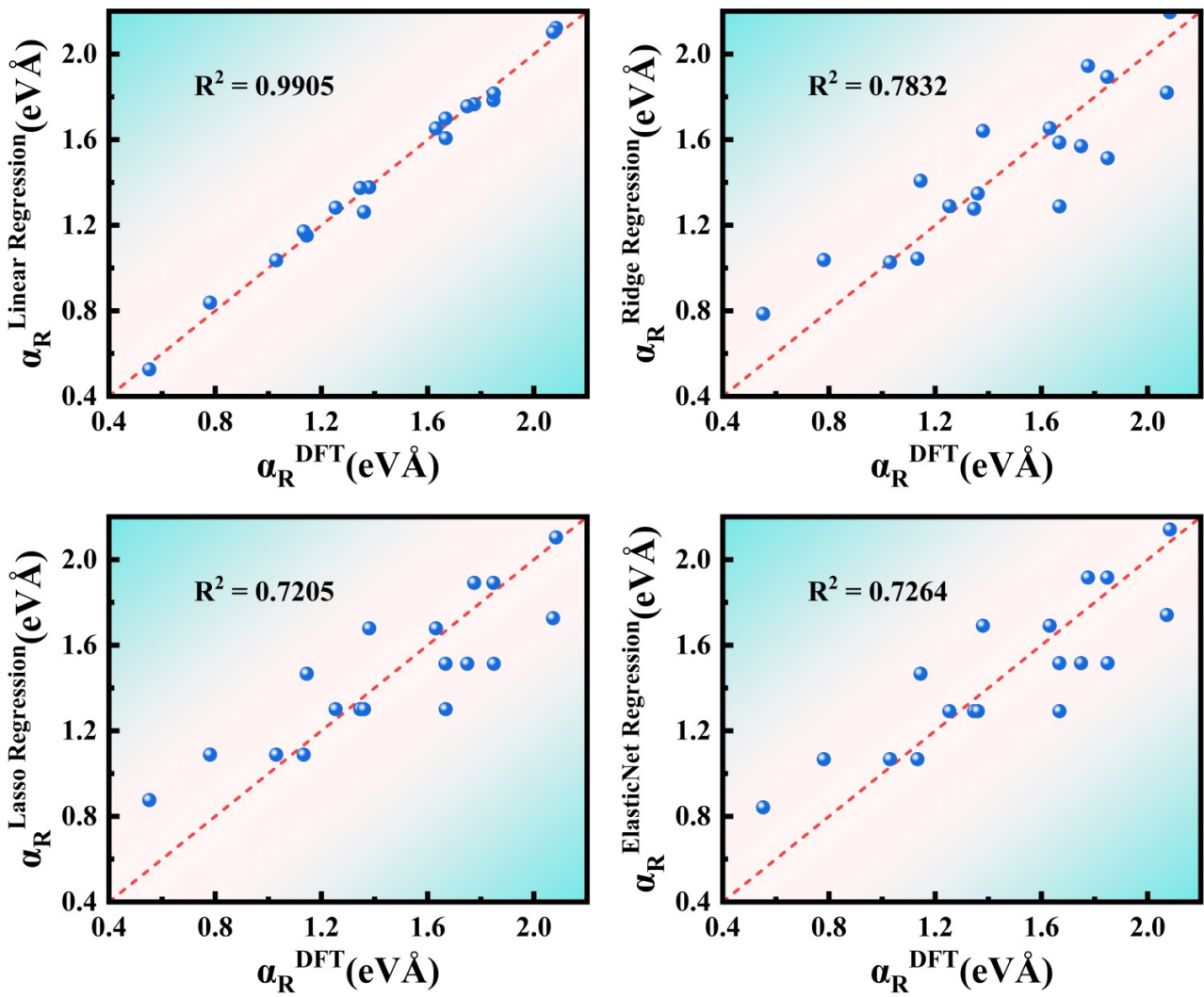


Figure S7. The comparison between the calculated values of Rashba spin-orbit coupling strength α_R obtained from different models and the results calculated by DFT method.

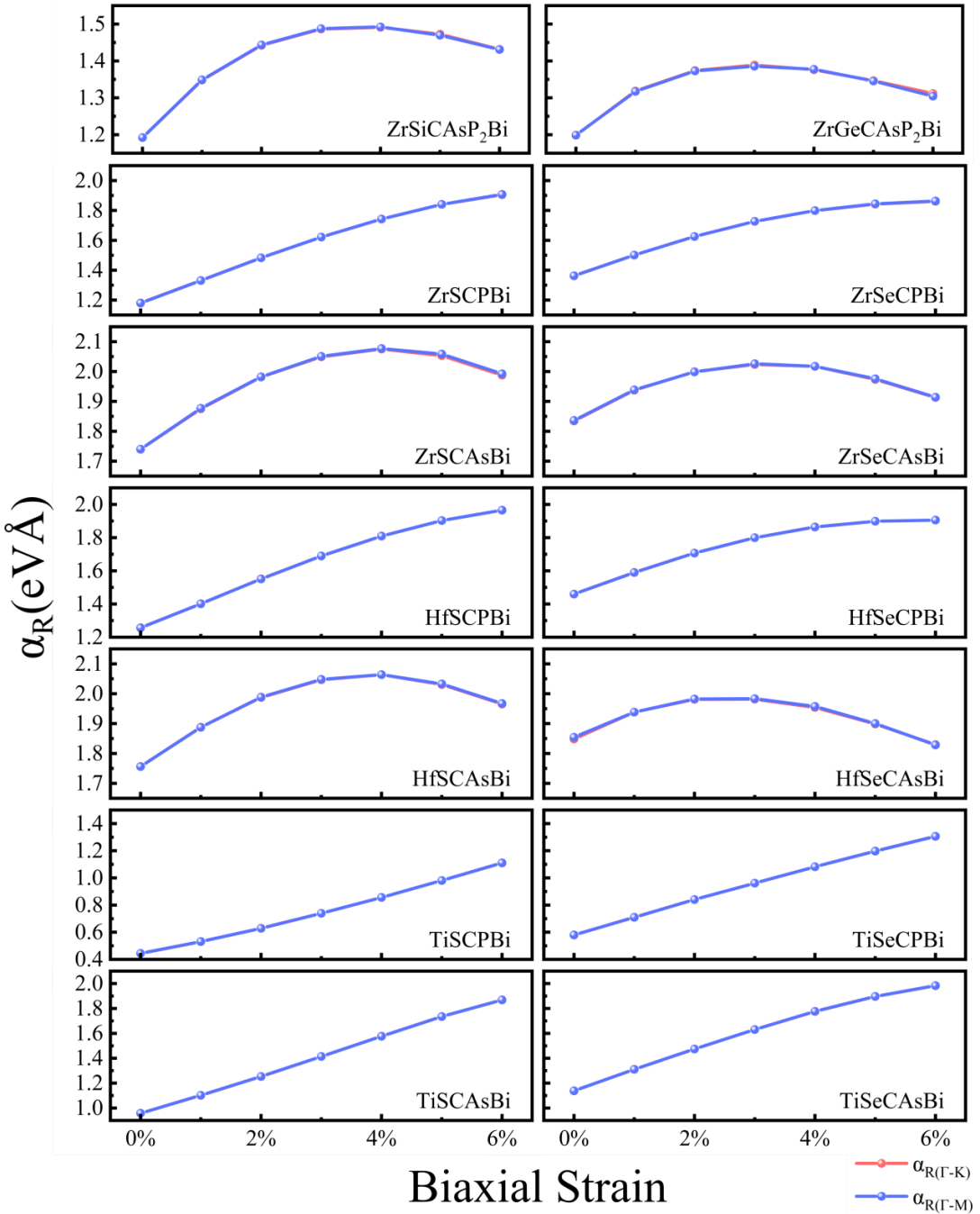


Figure S8. The variation of Rashba constant α_R with biaxial strain for several materials in MA_2Z_4 and MXAZ_2 systems.

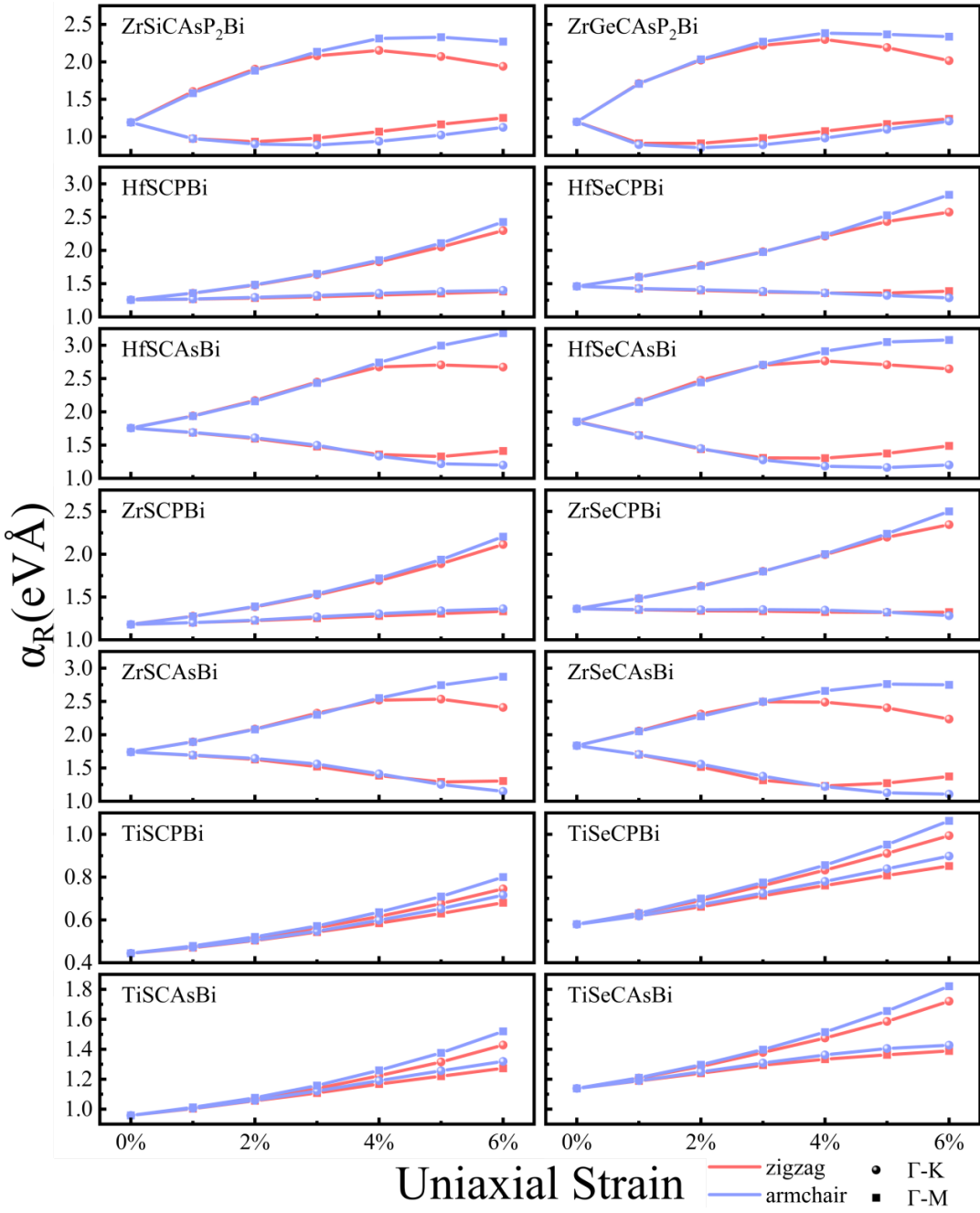


Figure S9. The variation of Rashba constant α_R with uniaxial strain for several materials in MA_2Z_4 and $MXAZ_2$ systems.

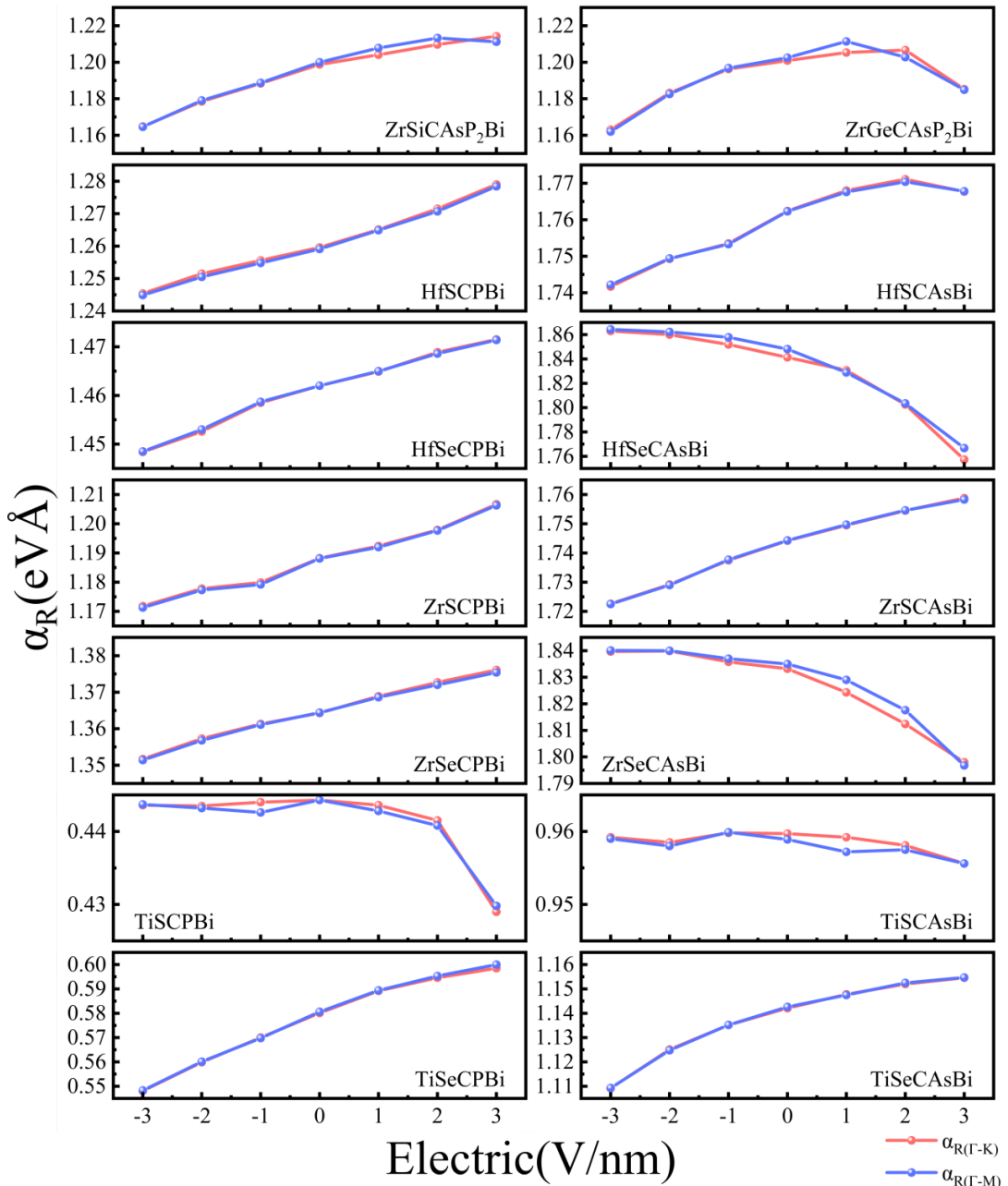


Figure S10. The variation of Rashba constant α_R with electric field for several materials in MA_2Z_4 and MXA_2Z_2 systems.

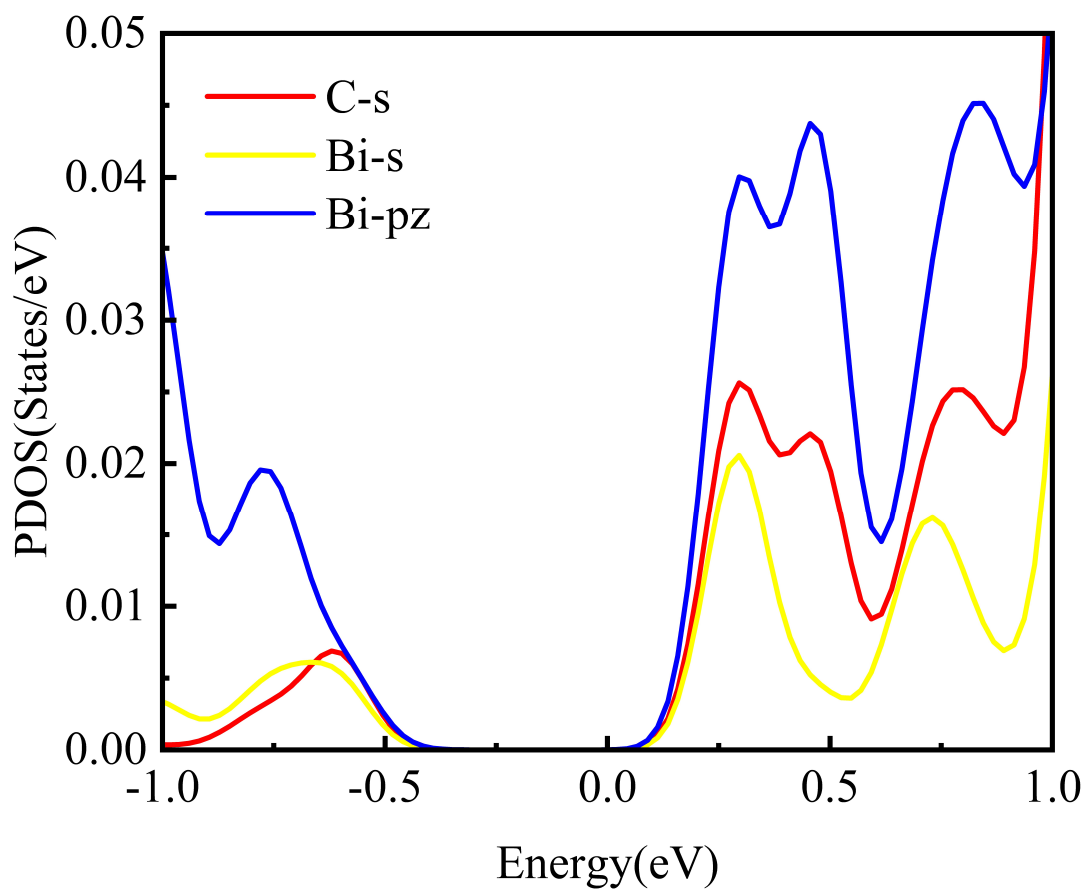


Figure S11. PDOS of the constituent atoms within the ZrSeCAsBi system.